New Journal of Physics
The open access journal at the forefront of physics

Deutsche Physikalische Gesellschaft DPG IOP Institute of Physics

PAPER • OPEN ACCESS

Sub-laser-cycle control of coupled electron–nuclear dynamics at a conical intersection

To cite this article: Maria Richter *et al* 2015 *New J. Phys.* **17** 113023

New Journal of Physics
The open access journal at the forefront of physics

Deutsche Physikalische Gesellschaft DPG
IOP Institute of Physics

Published in partnership with: Deutsche Physikalische Gesellschaft and the Institute of Physics

OPEN ACCESS

RECEIVED
17 June 2015

REVISED
3 September 2015

ACCEPTED FOR PUBLICATION
6 October 2015

PUBLISHED
6 November 2015

PAPER

Sub-laser-cycle control of coupled electron–nuclear dynamics at a conical intersection

Maria Richter[1,2], **Foudhil Bouakline**[1], **Jesús González-Vázquez**[3], **Lara Martínez-Fernández**[3], **Inés Corral**[3], **Serguei Patchkovskii**[1], **Felipe Morales**[1], **Misha Ivanov**[1,2,4], **Fernando Martín**[3,5,6] **and Olga Smirnova**[1]

[1] Max-Born-Institute, Max-Born-Strasse 2A, D-12489 Berlin, Germany
[2] Department of Physics, Imperial College London, South Kensington Campus, SW7 2AZ London, UK
[3] Departamento de Química, Módulo 13, Universidad Autónoma de Madrid, E-28049 Madrid, Spain
[4] Department of Physics, Humboldt University, Newtonstr. 15, D-12489 Berlin, Germany
[5] Instituto Madrileño de Estudios Avanzados en Nanociencia (IMDEA Nano), Cantoblanco, E-28049 Madrid, Spain
[6] Condensed Matter Physics Center (IFIMAC), Universidad Autónoma de Madrid, E-28049 Madrid, Spain

E-mail: Maria.Richter@mbi-berlin.de

Keywords: sub-femtosecond laser control, molecular dynamics, conical intersection, nonadiabatic effects

Supplementary material for this article is available online

Abstract

Nonadiabatic processes play a fundamental role in the understanding of photochemical processes in excited polyatomic molecules. A particularly important example is that of radiationless electronic relaxation at conical intersections (CIs). We discuss new opportunities for controlling coupled electron–nuclear dynamics at CIs, offered by the advent of nearly single-cycle, phase-stable, mid-infrared laser pulses. To illustrate the control mechanism, a two-dimensional model of the NO_2 molecule is considered. The key idea of the control scheme is to match the time scale of the laser field oscillations to the characteristic time scale of the wave packet transit through the CI. The instantaneous laser field changes the shape and position of the CI as the wave packet passes through. As the CI moves in the laser field, it 'slices' through the wave packet, sculpting it in the coordinate and momentum space in a way that is sensitive to the carrier-envelope phase of the control pulse. We find that the electronic coherence imparted on the sub-laser-cycle time scale manifests during much longer nuclear dynamics that follow on the many tens of femtosecond time scale. Control efficiency as a function of molecular orientation is analyzed, showing that modest alignment is sufficient for showing the described effects.

1. Introduction

Not only monitoring, but also controlling molecular processes has always been one of the main goals in physics, chemistry and biology, as it opens the possibility for their guided manipulation. In particular, the advances in laser technology open up a steadily widening range of opportunities for coherent quantum control of molecular dynamics.

Already in the late 1980s, quantum control strategies have been suggested, including the 'coherent phase-control technique' by Brumer and Shapiro [1, 2], the 'pump–dump time delay control technique' by Tannor, Rice and Kosloff [3, 4], and the technique proposed by Bergmann and co-workers [5–7], which has become known as 'stimulated Raman adiabatic passage' (STIRAP).

Since these seminal works, impressive achievements in controlling molecular processes have been reported, exploring all kinds of different laser field parameters, such as intensity, frequency, pulse duration, etc. In particular, the method termed 'optimal control theory' (OCT) has extended the one-parameter control schemes by employing feedback learning algorithms to generate complex laser pulses that are shaped in both the time and frequency domain and which are designed to optimize a desired outcome of a given molecular reaction [8–12].

This adaptive-control scheme has now been applied to a variety of molecules to govern specified chemical processes [13–16].

We discuss new opportunities for controlling multidimensional coupled electron–nuclear dynamics, offered by the advent of nearly single-cycle, phase-stable, mid-infrared (MIR) laser pulses. The key idea of the specific control scheme discussed here is to match the time scale of the laser field oscillations to the characteristic time scale of the wave packet passage through a conical intersection (CI) [17–19]. The instantaneous laser field changes the shapes of the intersecting potential energy surfaces (PESs) as the wave packet moves through the CI region. As a consequence, following the oscillations of the field, the intersection point moves in the nuclear coordinate space and 'slices' through the passing nuclear wave packet, thereby sculpting it in the coordinate and momentum space. This leads to two consequences. First, the laser pulse changes the wave packet transfer through the CI, and thus the branching ratio, in a way that is sensitive to the carrier-envelope phase (CEP) of the control pulse. Second, further wave packet passages through the CI, long after the end of the laser pulse, retain the memory of the control pulse. Both the shapes of the nuclear wave packets on each PES and the relative phase between them control the field-free dynamics on the many tens of femtosecond time scale. Thus the electronic coherence imparted on the sub-laser-cycle time scale manifests during much longer nuclear dynamics that follow.

Coupled electron–nuclear dynamics at CIs, and in particular their control with a laser field, is a rich and active field of research. In the following, we give a brief overview of different laser control schemes that have been developed to manipulate non-adiabatic dynamics at CIs. Especially for the complex photodynamics in larger molecules, which are complicated by the numerous non-adiabatic couplings between the various electronic states, OCT has been demonstrated both experimentally and theoretically to be an effective tool to guide the temporal evolution of a molecular system via a CI towards a desired target state (chemical product) by means of the feedback-optimized, shaped laser pulses [20–26].

Similar works have been performed involving the $S_2 \rightarrow S_1$ internal conversion process in pyrazine, which is a benchmark system for non-adiabatic dynamics at CIs (see e.g. [27–30] and references therein) and subject of numerous, diverse control studies [31–34]. Using pyrazine as an example, a general approach for suppressing radiationless transitions has been proposed [35, 36], combining OCT with the concept of electronically localized eigenstates of strongly vibronically coupled systems, to populate a stable superposition state. It has been shown that the formation of such a stationary state allows the suppression of the radiationless decay for extended time periods on the nanosecond time scale. Pyrazine has also been employed [37, 38] to examine the possibility of extensive control based on the concept of overlapping resonances [39–41], to either minimize or maximize the population that undergoes the radiationless transition.

Another route for controlling wave packet dynamics at CIs or avoided crossings is based on the observation that the dynamics is particularly sensitive to changes of the topography of the PESs close to the coupling region. It has been shown that molecular processes can be controlled with short, intense IR fields via the nonresonant dynamic Stark effect (NRDSE) [42–53], where the IR photons are not in resonance with an electronic transition in the molecule. Both experimentally and theoretically it has been demonstrated that this effect can be used to control the photodissociation branching ratio at the avoided crossing present in the IBr molecule [54–57]. The pulse-dependent modifications of the potential energy curves induced by the NRDSE manipulate the wave packet velocity at the crossing, which, in turn, affects the Landau–Zener transition probability [50–52]. To date the NRDSE scheme has been successfully employed to control different molecular proccesses in various systems [58–63]. Recently it has been shown that the NRDSE can modify the topography of the PESs in pyrazine, using a four-dimensional [64] and a full 24-dimensional [65] model. Here, the CI is shifted away from the Franck-Condon region, where a new minimum is created, localized on the S_2 PES. As a consequence, the wave packet is trapped on the S_2 PES, where it stays for a much longer period than the natural S_2 lifetime.

As relatively long, many-cycle pulses have been used in the majority of the laser control studies, the influence of the CEP of the pulse on the nuclear wave packet dynamics at a CI has not been subject of particular interest until recent work presented in [66]. In [66], the effect of a few-cycle, MIR control pulse on the population dynamics mediated by a CI has been examined. The control pulse acts on the molecule just *before* the internal conversion process at the CI takes place. Changing the CEP of the control pulse changes the phase of the wave packet approaching the coupling region. The interplay between this phase and that imprinted by the non-adiabatic coupling now defines the path through the CI and thus the final branching ratio.

In comparison, in the present work, we analyze how a nearly single-cycle IR pulse affects the nuclear wave packet *while* it propagates through the CI region. To illustrate the idea of control via a laser-driven, 'sculpting' intersection, we consider an example of the NO_2 molecule within a two-dimensional (2D) approximation. In this molecule, the transit through the $1^2A_1/1^2B_2$ CI is very fast, taking only about $\tau_{CI} \sim 6$ fs. The presented calculations correspond to a particular, favorable orientation of the molecule. However, complementary calculations for different spatial orientations of the molecule (not depicted here) show that already a moderate

molecular alignment distribution of $\cos^2\alpha \approx 0.5$ is sufficient to observe the effect of the control pulse discussed here.

Already in 2010, Arasaki *et al* have reported on the effect of a control pulse on the wave packet dynamics at the $1^2A_1/1^2B_2$ CI in NO_2 [67, 68]. They have studied the modifications of the PESs induced by a half-cycle, long-wavelength infrared laser pulse with a wavelength of $\lambda = 12.4$ μm, corresponding to a laser period of $T_l \approx 41.4$ fs. In this case, the intersection is shifted away in the nuclear coordinate space from its field-free position for the entire time interval, τ_{CI}, in which the wave packet passes through the (field-free) coupling region. Therefore the wave packet largely 'misses' the non-adiabatic coupling region while propagating on the excited adiabatic state, resulting in a suppression of the radiationless decay in NO_2.

Here, we use a control field with a wavelength of $\lambda = 1600$ nm. Importantly, the period of this field ($T_l \approx 5.3$ fs) approximately matches the CI transit time τ_{CI}. Using the laser pulse centered at $\lambda = 1600$ nm and with a FWHM (full width at half maximum) duration of 6 fs ($\sim\tau_{CI}$), we strongly modify the wave packet dynamics over the subsequent few tens of femtoseconds by re-shaping the nuclear wave packet during its CI passage. The wave packet dynamics is noticeably different when the CEP of the control pulse is changed by $\pi/4$, corresponding to a control on the sub-femtosecond time scale.

We note that similar CEP control scenarios, using few-cycle (up to single-cycle) MIR pulses with cycle durations comparable to the time scale of the nuclear dynamics, have been previously implemented for the diatomic molecules NaI [69], LiF [70, 71] and D_2 [72]. In these one-dimensional problems, the laser-induced motion of the avoided crossing point is parallel to the propagation direction of the nuclear wave packet. In contrast, in this work we have the situation that the intersection point moves mainly perpendicular relative to the nuclear wave packet motion, resulting in very different transition dynamics.

The paper is organized as follows. In section 2 we present the model and the computational methodology used in this work. The results are presented in section 3, together with a discussion of the CEP-dependent population dynamics at the CI and an analysis of the mechanism behind the laser control. Our conclusions are given in section 4.

2. Computations

2.1. Electronic structure calculations

The ultrafast (femtosecond time scale) electronic relaxation of NO_2 via non-adiabatic transitions has been widely explored both theoretically and experimentally [73–89].

Extensive static quantum chemical calculations of NO_2 PESs, using a broad spectrum of theoretical approaches, covering single- and multiconfigurational schemes and dynamically correlated and uncorrelated methods are available in the literature [75, 78, 82, 90–117]. These calculations serve as a basis for the dynamical simulations and have ultimately guided the interpretation of the complex spectroscopical features of NO_2. The topological landscape of the 1^2A_1 ground state PES, disregarding dissociation or peroxy isomerization regions, is characterized by a global minimum occurring at an N–O equilibrium distance of $R_e = 1.154 - 1.23$ Å and at an O–N–O bond angle of $\theta = 132.7° - 137.5°$ (the experimental values are $R_e = 1.193 - 1.197$ Å and $\theta = 133.2° - 134.2°$ [118–123]). The 1^2A_1 state is predicted to intersect with the upper electronic state 1^2B_2 0.96 − 1.48 eV above the global minimum at $R_e = 1.242 - 1.311$ Å and $\theta = 106.6° - 114°$, leading to a $1^2A_1/1^2B_2$ CI (the experimental values are $R_e = 1.246$ Å, $\theta = 103.1°$, and $T_e = 1.21$ eV [124]), corresponding to the energetic minimum of the CI seam. The CI is located in the vicinity of the minimum of the 1^2B_2 PES ($R_e = 1.212 - 1.373$ Å and $\theta = 101.0° - 102.8°$; expt.: $R_e = 1.244$ Å and $\theta = 102.6°$ [125]). A substantial energy barrier separates the 1^2B_2 minimum from a crossing with the 2^2A_1 state, almost at the linear geometry [78]. Also at linearity, and high above the 1^2B_2 minimum, the 1^2B_1 state is calculated to be degenerate with the electronic ground state 1^2A_1 [78, 126, 127]. The number of interstate crossings increases with the excitation energy, increasing the complexity of the high-lying excited PESs.

This work focusses on studying the effect of a control laser pulse on the wave packet dynamics at a CI, rather than on a global description of the dynamics of NO_2. We therefore use a reduced-dimensionality model for the NO_2 PESs, comprising the two coordinates essential for the description of the internal conversion funnel [128]. These coordinates, which define the branching space of a CI, are the gradient difference and derivative coupling vectors. In the case of the NO_2 molecule they correspond to the bending and the asymmetric stretch modes, θ and r_a, respectively, where r_a is half the difference between the two N–O distances (R_{NO}). The third internal degree of freedom, the symmetric stretch coordinate, was constrained to its value at the MR-CISD (multireference configuration interaction with all single and double excitations) geometry of the CI (details below). Another reason for choosing the reduced-dimensionality model is the numerical cost of the 3D calculations, given that a large number of simulations for different laser parameters is required to fully analyze the physics underlying the discussed control scenario.

Table 1. Minimum and CI optimized geometries and energies of the 1^2A_1 and 1^2B_2 states at these points of the PESs relative to the 1^2A_1 ground state minimum.

	R_{NO} (Å)	θ (degrees)	1^2A_1 energy (eV)/(Hartree)	1^2B_2 energy (eV)/(Hartree)
1^2A_1 minimum	1.203	133.7	0.00/0.000	3.25/0.119
1^2B_2 minimum	1.265	101.8	1.86/0.068	1.20/0.044
$1^2A_1/1^2B_2$ CI	1.259	107.3	1.25/0.046	1.25/0.046

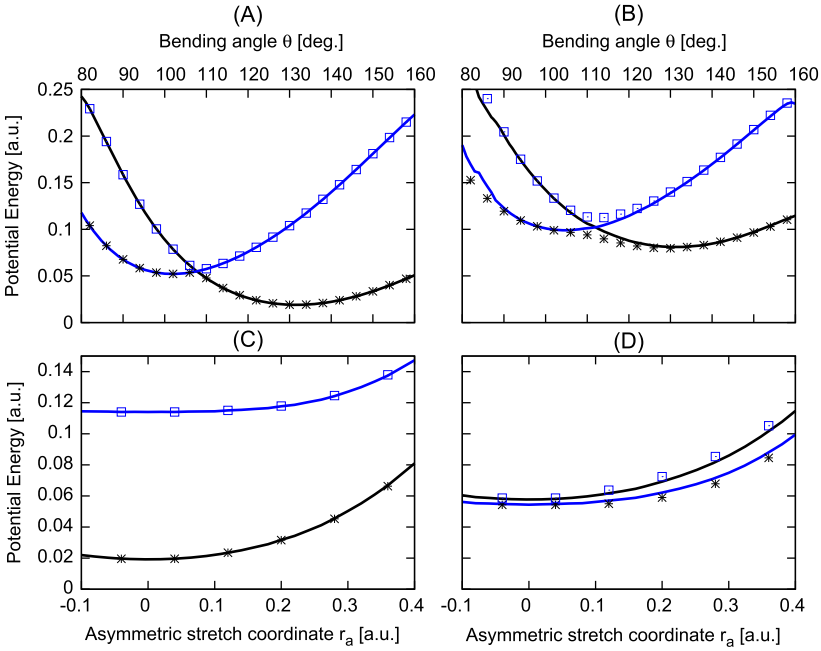

Figure 1. One-dimensional cuts of the adiabatic potential energy curves (PECs), corresponding to the states $1^2A'$ (asterisks) and $2^2A'$ (squares), and of the diabatic PECs, corresponding to the states 1^2A_1 (black solid line) and 1^2B_2 (blue solid line) for C_{2v} symmetry. (A) and (B): cuts along the bending angle θ at $r_a = 0$ a.u. (C_{2v} symmetry) (A), and at $r_a = 0.4$ a.u. (B). (C) and (D): cuts along the asymmetric stretch coordinate r_a (the curves are symmetric with respect to $r_a = 0$ a.u.) passing through the minimum of the $1^2A'$ state (C) and the CI geometry (D).

A multiconfigurational ansatz was used for the description of the degeneracy regions and excited state PESs. The initial reference wave functions were computed using the CASSCF method and the 6–311G* basis set. The calculations were carried out in C_s symmetry and state-averaged over the lowest two roots. Within the C_s symmetry point group, the C_{2v} states 1^2A_1 and 1^2B_2 belong to the same irreducible representation A' ($1^2A'$ and $2^2A'$), and can mix through the asymmetric stretch mode (r_a). The CASSCF active space consisted of 11 electrons in nine orbitals, correlating to the atomic 2p orbitals. The electronic energies were optimized using the MR-CISD approach, with CASSCF as the reference, employing the Columbus Quantum Chemistry Package [129–134]. Core (1s) orbitals were not correlated. Table 1 summarizes the calculated stationary points and interstate crossing of the 2D PESs. The MR-CISD minima and CI geometries are very close to the experimental structures obtained in [118–125] and also in close coincide with previous MR-CID results [75, 78, 91, 95].

Adiabatic potential energies and dipole moments were calculated on a product grid along the bending angle θ(O–N–O) (80°–180°, step size $\Delta\theta = 1°$) and the asymmetric stretch coordinate r_a (−0.6 to +0.6 a.u., step size $\Delta r_a = 0.02$ a.u.). The symmetric stretch coordinate was fixed at $\tilde{r}_s = 1.259$ Å (its value at the CI geometry). Figure 1 illustrates one-dimensional cuts of the calculated potentials.

The quantum wave packet dynamics calculations were performed using the quasi-diabatic representation [135, 136] (see figure 1). The use of diabatic PESs avoids the treatment of divergent kinetic energy couplings at the CI geometry, since the coupling is no longer described by the kinetic energy operator, but rather as a potential coupling—a smooth function of the nuclear coordinates θ and r_a. For the construction of diabatic states, a number of schemes based on different approaches have been developed, for an overview see [17]. For the present study, the diabatic electronic states were constructed using the orbital-based quasi-diabatization procedure that is implemented in MOLPRO 2009 [137, 138]. It relies on the minimization of the derivative

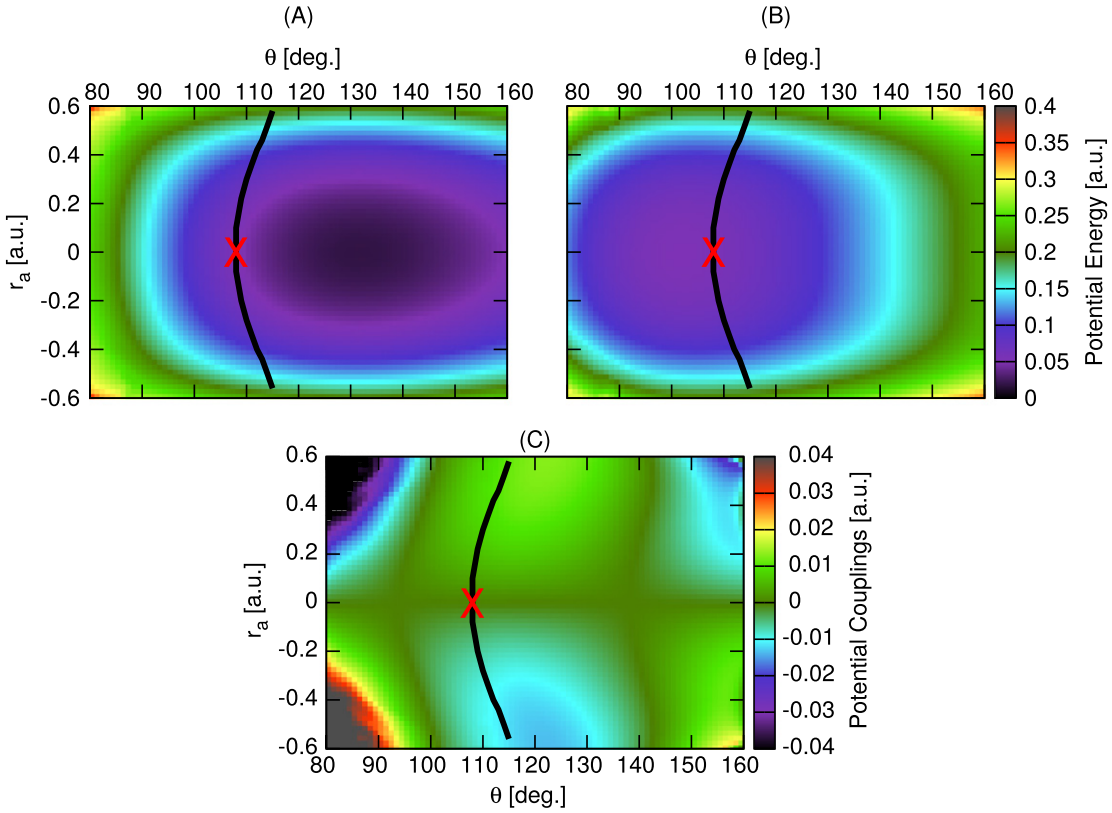

Figure 2. Two-dimensional diabatic potentials: (A) ground diabatic potential energy surface V_1^{d}, (B) excited diabatic potential energy surface V_2^{d}, (C) potential coupling surface V_{12}^{d}. The solid black line indicates the nuclear geometries at which the two diabatic PESs cross. The red cross indicates the CI geometry.

couplings by employing the condition of configurational smoothness of diabatic states. Starting from a suitable reference geometry, the diabatic electronic wave functions at neighboring geometries are determined by maximizing the overlap with the diabatic reference electronic wave function, usually the electronic eigenfunctions at equilibrium geometry, using a unitary transformation matrix. The solid lines in figure 1(A) depict the diabatization result for the system constrained to C_{2v} symmetry ($r_a = 0$ a.u.). As expected, the adiabatic and diabatic curves are superimposed, since the potential coupling vanishes in C_{2v} symmetry. For bending angles larger than that corresponding to the CI geometry ($\theta > 107.3°$), the ground adiabatic state, $1^2A'$, coincides with the 1^2A_1 state, while the excited adiabatic state, $2^2A'$, coincides with the 1^2B_2 state. For $\theta < 107.3°$ the situation is reversed. In comparison, figure 1(B) depicts the adiabatic and diabatic curves for $r_a \neq 0$ a.u.. The adiabatic and diabatic curves are no longer entirely superimposed. In the vicinity of the CI point, where the adiabatic states avoid each other, the diabatic curves cross. Panels 1(C), (D) represent potential energy curves along the asymmetric stretch coordinate. The curves pass through the minimum of the 1^2A_1 state (C) and the CI geometry (D). In figure 1(C), the states are well separated and the adiabatic and diabatic curves coincide. In figure 1(D), the two curves are slightly different away from the C_{2v} symmetry.

Finally, figure 2 shows the 2D diabatic PESs and the potential coupling surface. The solid black line in the panels 2(A)–(C) indicates nuclear geometries at which the two diabatic surfaces intersect. The CI (marked by the red cross) is located at the point of the intersection between the two diabatic PESs, where the potential coupling vanishes ($r_a = 0$ a.u. and $\theta \sim 107°$).

2.2. Wave packet dynamics calculations

The total wave function describing the system, $\Psi(\boldsymbol{r}, \boldsymbol{R})$, is expanded in the basis of the two coupled diabatic electronic states, $\varphi_1(\boldsymbol{r}; \boldsymbol{R})$ and $\varphi_2(\boldsymbol{r}; \boldsymbol{R})$,

$$\Psi(\boldsymbol{r}, \boldsymbol{R}, t) = \chi_1^{\mathrm{d}}(\boldsymbol{R}, t)\varphi_1(\boldsymbol{r}; \boldsymbol{R}) + \chi_2^{\mathrm{d}}(\boldsymbol{R}, t)\varphi_2(\boldsymbol{r}; \boldsymbol{R}). \quad (1)$$

Here χ_i^{d} $(i = 1, 2)$ is the vibrational wave function associated with state i, $\boldsymbol{r}$ stands for all electronic coordinates, and $\boldsymbol{R}$ designates nuclear coordinates, i.e., the asymmetric stretch coordinate r_a and the bending angle θ.

We solve the following system of coupled equations:

$$
\begin{aligned}
\mathrm{i}\hbar\frac{\partial}{\partial t}\begin{pmatrix}\chi_1^{\mathrm{d}}(\boldsymbol{R},\,t)\\ \chi_2^{\mathrm{d}}(\boldsymbol{R},\,t)\end{pmatrix} &= \left[\boldsymbol{T}^{\mathrm{d}}+\boldsymbol{V}^{\mathrm{d}}+\boldsymbol{W}^{\mathrm{d}}\right]\begin{pmatrix}\chi_1^{\mathrm{d}}(\boldsymbol{R},\,t)\\ \chi_2^{\mathrm{d}}(\boldsymbol{R},\,t)\end{pmatrix}\\
&= \left[\begin{pmatrix} T^{\mathrm{d}}\left(\boldsymbol{R},\frac{\partial}{\partial\boldsymbol{R}}\right) & 0\\ 0 & T^{\mathrm{d}}\left(\boldsymbol{R},\frac{\partial}{\partial\boldsymbol{R}}\right)\end{pmatrix}+\begin{pmatrix}V_1^{\mathrm{d}}(\boldsymbol{R}) & V_{12}^{\mathrm{d}}(\boldsymbol{R})\\ V_{12}^{\mathrm{d}}(\boldsymbol{R}) & V_2^{\mathrm{d}}(\boldsymbol{R})\end{pmatrix}\right.\\
&\quad\left.-\begin{pmatrix}\boldsymbol{d}_1^{\mathrm{d}}(\boldsymbol{R}) & \boldsymbol{d}_{12}^{\mathrm{d}}(\boldsymbol{R})\\ \boldsymbol{d}_{12}^{\mathrm{d}}(\boldsymbol{R}) & \boldsymbol{d}_2^{\mathrm{d}}(\boldsymbol{R})\end{pmatrix}\cdot\boldsymbol{E}(t)\right]\begin{pmatrix}\chi_1^{\mathrm{d}}(\boldsymbol{R},\,t)\\ \chi_2^{\mathrm{d}}(\boldsymbol{R},\,t)\end{pmatrix},
\end{aligned}
\tag{2}
$$

where T^{d} denotes the kinetic energy operator (see below). V_1^{d} (V_2^{d}) and $\boldsymbol{d}_1^{\mathrm{d}}$ ($\boldsymbol{d}_2^{\mathrm{d}}$) are the diabatic PES and the diabatic permanent dipole moment of state 1 (2), respectively. V_{12}^{d} and $\boldsymbol{d}_{12}^{\mathrm{d}}$ describe the potential coupling and the diabatic transition dipole moment between the two diabatic electronic states φ_1 and φ_2, respectively. $\boldsymbol{E}(t) = E_0 f(t)\cos(\omega t+\phi_{\mathrm{CEP}})\boldsymbol{e}_y$ defines the laser pulse, where E_0 is the peak electric field strength, $f(t)$ is the Gaussian pulse envelope, ω the field frequency, ϕ_{CEP} controls the CEP of the pulse, and $\boldsymbol{e}_y$ denotes the unit vector along the y-axis. The propagation of the vibrational wave packets is performed entirely in internal coordinates. The spatial orientation of the molecule in the calculations is therefore determined only by the elements of the laser-molecule coupling matrix, $\boldsymbol{d}^{\mathrm{d}}\cdot\boldsymbol{E}$. The molecule is placed in the x–y plane, where the x-axis coincides with the bisector of the bending angle θ. At this orientation, for symmetry reasons, only the y component of the transition dipole moment is non-zero for C_{2v} configurations ($r_{\mathrm{a}} = 0$ a.u.) of the molecule. The proposed control scheme suggests to irradiate the molecule while the vibrational wave packet passes through the CI, which occurs for C_{2v} configuration. Hence, only the y component of the control field contributes to the laser coupling. Molecules with different orientations with respect to the laser polarization direction will be affected similarly by the control pulse, but the strength of the effect depends on the projection of the electric field vector on the y axis of the molecule-fixed frame. Additional results obtained for different orientations of the molecule (not depicted here) show that already a moderate molecular alignment distribution of $\cos^2\alpha \approx 0.5$ is sufficient to observe the effect of the control pulse discussed here. Such moderate alignment distribution is expected to be generated by the excitation pulse. The reduced 2D vibrational kinetic energy operator, expressed in terms of the asymmetric stretch coordinate r_{a} and the bending angle θ, reads

$$
\begin{aligned}
T^{\mathrm{d}} = &-\frac{\hbar^2}{4\mu}\frac{\partial^2}{\partial r_{\mathrm{a}}^2}+\frac{\hbar^2}{4m_{\mathrm{N}}}\cos\theta\,\frac{\partial^2}{\partial r_{\mathrm{a}}^2}\\
&-\frac{\hbar^2}{2}\left(\frac{1}{\mu\left(\tilde{r}_{\mathrm{s}}+r_{\mathrm{a}}\right)^2}+\frac{1}{\mu\left(\tilde{r}_{\mathrm{s}}-r_{\mathrm{a}}\right)^2}\right)\left(\frac{\partial^2}{\partial\theta^2}+\cot\theta\,\frac{\partial}{\partial\theta}\right)\\
&+\frac{\hbar^2}{2m_{\mathrm{N}}}\frac{1}{\tilde{r}_{\mathrm{s}}^2-r_{\mathrm{a}}^2}\left[\cos\theta\left(\frac{\partial^2}{\partial\theta^2}+\cot\theta\,\frac{\partial}{\partial\theta}\right)+\left(\frac{\partial^2}{\partial\theta^2}+\cot\theta\,\frac{\partial}{\partial\theta}\right)\cos\theta\right]\\
&+\frac{\hbar^2}{2m_{\mathrm{N}}}\left[\frac{r_{\mathrm{a}}}{\tilde{r}_{\mathrm{s}}^2-r_{\mathrm{a}}^2}\frac{\partial}{\partial r_{\mathrm{a}}}+\frac{\partial}{\partial r_{\mathrm{a}}}\frac{r_{\mathrm{a}}}{\tilde{r}_{\mathrm{s}}^2-r_{\mathrm{a}}^2}\right]\left(\sin\theta\,\frac{\partial}{\partial\theta}+\cos\theta\right)\\
&-\frac{\hbar^2}{2m_{\mathrm{N}}}\frac{r_{\mathrm{a}}^2+\tilde{r}_{\mathrm{s}}^2}{\left(\tilde{r}_{\mathrm{s}}^2-r_{\mathrm{a}}^2\right)^2}\cos\theta+\frac{\hbar^2}{m_{\mathrm{N}}}\frac{1}{\tilde{r}_{\mathrm{s}}^2-r_{\mathrm{a}}^2}\cos\theta.
\end{aligned}
\tag{3}
$$

Here $\mu = m_{\mathrm{N}}m_{\mathrm{O}}/(m_{\mathrm{N}}+m_{\mathrm{O}})$ with m_{N} and m_{O} denoting the mass of the nitrogen and oxygen atoms, respectively. A detailed description of the construction of this specific, reduced-dimensionality kinetic energy operator is beyond the scope of this work [139]. A general recipe for the construction of a molecular kinetic energy operator in curvilinear coordinates, including molecular systems subject to constraints, is extensively described in [140–142].

We employ the direct product discrete variable representation (DVR) method for solving the time-dependent Schrödinger equation (2). For the asymmetric stretch coordinate r_{a} we use the Colbert–Miller sine DVR [143], while for the bending angle θ, we utilize a Gauss–Legendre DVR. We use $N_{r_{\mathrm{a}}} = 41$ points for the r_{a}—grid, which ranges from -0.57 to $+0.57$ a.u., and $N_\theta = 90$ points for the θ—grid, ranging from 61° to 179°. The time-dependent coupled equations (2) are then propagated by a split-operator method, using a time step of $\Delta\mathrm{t} = 0.024$ fs. At each time step, we also calculate the adiabatic ground and excited nuclear wave functions, $\chi_{\mathrm{g}}^{\mathrm{ad}}$

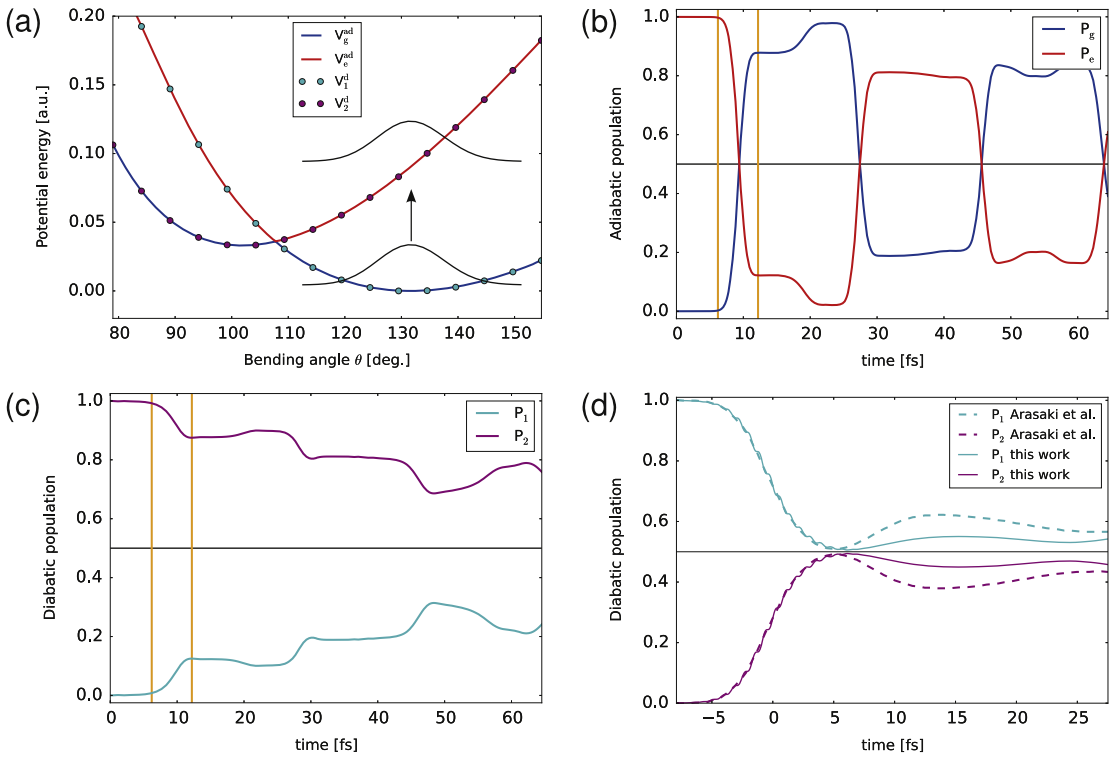

Figure 3. (a)–(c) Field-free population dynamics. (a) Sketch of initialization of field-free dynamics. Cuts of the potential energy surfaces along the bending angle θ at $r_a = 0$ a.u. of the ground (blue solid line) and excited adiabatic state (red solid line), and of the diabatic state 1 (cyan dots) and 2 (magenta dots). At $t = 0$ fs, the lowest vibrational state (solid line) of the electronic ground state is placed on the upper adiabatic surface as indicated by the arrow. (b) Population evolution of the ground (blue) and excited adiabatic state (red). (c) Population evolution of diabatic state 1 (cyan) and 2 (magenta). The vertical orange lines in (b) and (c) highlight the start and end time of the first CI passage. (d) Comparison between our 2D results and the 3D results presented in figure 2 of [85] (Reprinted with permission from [85]. Copyright [2010], AIP Publishing LLC.) for the diabatic population evolution upon excitation with a Gaussian pump pulse centered at $t = 0$ fs and a FWHM of 8 fs. As different *ab initio* potential energy surfaces are used in both works, we have adjusted the pump pulse wavelength to $\lambda = 513$ nm, compared to $\lambda = 400$ nm used in [85], to transfer the same amplitude to the excited state. The subsequent field-free population evolution exhibits nearly the same characteristic time scale in both cases.

and χ_e^{ad}, from the diabatic nuclear wave functions:

$$\begin{pmatrix} \chi_g^{ad}(\boldsymbol{R}, t) \\ \chi_e^{ad}(\boldsymbol{R}, t) \end{pmatrix} = \boldsymbol{M} \begin{pmatrix} \chi_1^{d}(\boldsymbol{R}, t) \\ \chi_2^{d}(\boldsymbol{R}, t) \end{pmatrix}, \tag{4}$$

where matrix $\boldsymbol{M}$ diagonalizes the diabatic potential energy matrix:

$$\boldsymbol{M} \begin{pmatrix} V_1^{d}(\boldsymbol{R}) & V_{12}^{d}(\boldsymbol{R}) \\ V_{12}^{d}(\boldsymbol{R}) & V_2^{d}(\boldsymbol{R}) \end{pmatrix} \boldsymbol{M}^{-1} = \begin{pmatrix} V_g^{ad}(\boldsymbol{R}) & 0 \\ 0 & V_e^{ad}(\boldsymbol{R}) \end{pmatrix}. \tag{5}$$

3. Results and discussion

3.1. Population dynamics

We initialize the coupled electron–nuclear wave packet dynamics at $t = 0$ fs by placing the lowest vibrational state of the electronic ground state on the upper adiabatic surface, equivalent to an instantaneous, complete Franck-Condon excitation of the molecular system, see figure 3(a).

Figure 3(b) shows the ensuing time evolution of the population of the two adiabatic states, $P_i(t) = |\chi_i^{ad}(t)|^2$ with $i = \{g, e\}$. The nuclear wave packet immediately starts to propagate towards smaller bending angles on the upper adiabatic surface. After approximately 6 fs it starts to encounter the CI region for the first time. While passing the coupling region, we can observe a strong non-adiabatic transition into the ground adiabatic state, leading to an increase of the electronic ground state population in the time interval from 6 to 12 fs, see figure 3(b). The part of the nuclear wave packet that did not hop on the lower adiabatic surface during the CI passage, but remained on the upper one, reaches its turning point first, where it reflects, and then propagates back towards the coupling region. The ensuing non-adiabatic transition during this second CI passage leads to

the second increase of the population of the ground adiabatic state between 15.5 and 21.5 fs. The nuclear wave packet evolving on the lower adiabatic surface, re-encounters the CI region later at $t \sim 25$ fs. During this CI passage, a substantial part of the nuclear wave packet is transferred back into the excited adiabatic state, leading to the significant drop of the ground state population. Figure 3(b) shows that the strong non-adiabatic transitions, which are accompanied by substantial population transfers between the two coupled states, occur with a period of approximately 18 fs.

The strong non-adiabatic transitions observed here, reflect the diabatic-like behavior of the field-free dynamics of NO_2. Figure 3(c) shows the time evolution of the population of the two diabatic electronic states, $P_j(t) = |\chi_j^{\mathrm{d}}(t)|^2$ with $j = \{1, 2\}$. The smooth time-dependence of the diabatic population illustrates the diabatic-like dynamics: Upon excitation, the nuclear wave packet mainly oscillates on the excited diabatic surface, V_2^{d}, with moderate population transfer between the two diabatic states, due to their moderate coupling (see figure 2(C)).

As we use a reduced-dimensionality (2D) model of NO_2, it is worthwhile to compare the dynamics described here with that obtained for a full three dimensional treatment of the problem. For that we have performed calculations similar to those presented by Arasaki *et al* in figure 2 of [85], obtaining the population evolution of the two diabatic states upon the interaction with a pump pulse. The results are shown in figure 3(d). Since we employ different *ab initio* PESs for the two electronic states, we have adjusted the pump pulse parameters (frequency and intensity) so that the same amplitude is transferred to the excited state by the pump. We find that the qualitative behavior of the subsequent field-free population evolution, including the first two passages through the CI, is in very good agreement. In particular, the population dynamics obtained by us, on the one hand, and Arasaki *et al* [85], on the other hand, exhibit nearly the same characteristic time scales.

As already mentioned above, the characteristic time, τ_{CI}, that it takes the nuclear wave packet to pass through the coupling region, is only $\tau_{\mathrm{CI}} \approx 6$ fs. This is indicated by the vertical orange lines in the panels 3(b) and (c), highlighting the start and the end time of the first CI passage. The time scale of the oscillations of a field with a wavelength of 1600 nm, corresponding to a period of $T_{\mathrm{l}} \approx 5.3$ fs, is thus comparable to this transit time τ_{CI}. Hence, we use a 1600 nm control pulse with a FWHM of 6 fs and a peak intensity of 5.6×10^{13} W cm^{-2}, see figure 4(a). Importantly, we apply the ultrashort laser pulse in the same time interval, in which the nuclear wave packet passes through the CI region for the first time ($t \sim 6$–12 fs), as indicated by the vertical orange lines in figure 4(a).

It should be noted that for the specific control scheme discussed here, it is preferable to excite the system by a short, sudden kick, generating a coherent, well-localized initial wave packet on the upper state. This way the CEP-dependent coherence imparted by the subsequent control pulse manifests during much longer dynamics that follow. Thus, an ultrashort excitation pulse is desirable. For the sake of clarity, we initialize the wave packet dynamics by means of a fictitious delta excitation. However, thanks to the continuous effort dedicated to the generation of ever-shorter light pulses, nowadays, single-cycle and even sub-cycle pulses can be generated for a wide range of central carrier frequencies using different state-of-the-art techniques [144–147], such as waveform synthesizers. We have repeated our calculations for a single-cycle pump pulse, resonant with the 1^2A_1 to 1^2B_2 transition at the 1^2A_1 equilibrium geometry and a peak intensity of 2.6×10^{13} W cm^{-2} (for such a short pump, excitation is still a nearly linear function of intensity), with virtually identical results (not depicted here). In case of substantially longer excitation pulses, additional effects induced by the overlap of the pump and control pulse need to be considered.

Panel 4(b) shows the laser-modified time evolution of the adiabatic population of the two states. We notice two things: (i) the first population transfer at the CI is strongly modified by the laser pulse, and (ii) the second and subsequent population transfers at the CI are largely suppressed, even though the pulse is off at $t \sim 18$ fs. The results shown in figure 4(b) correspond to calculations using a pulse with a CEP of $\phi_{\mathrm{CEP}} = 0$. In panel 4(d), we present the evolution of the laser-modified population of the excited adiabatic state obtained with the same pulse, but different CEP: $\phi_{\mathrm{CEP}} = \pi/4$ (black curve), and $\phi_{\mathrm{CEP}} = \pi/2$ (green curve), see panel 4(c). Our results show that the dynamics at the CI are sensitive to the CEP of the pulse, revealing the potential of its sub-cycle, and thus sub-femtosecond control.

The significant modification of the population dynamics indicates strong laser-induced changes of the PESs and couplings. To gain a better insight into the process responsible for this CEP-dependent molecular response, it is useful to study the laser-induced modifications of the nuclear wave packet, as can be seen in the next section.

3.2. Wave packet dynamics

Figure 5 shows the evolution of the nuclear probability density, in the absence of the control field, integrated over the bending angle θ, i.e., as a function of the asymmetric stretch coordinate r_{a} and time t. Panel (a) corresponds to the upper adiabatic surface, and panel (b) to the lower adiabatic surface.

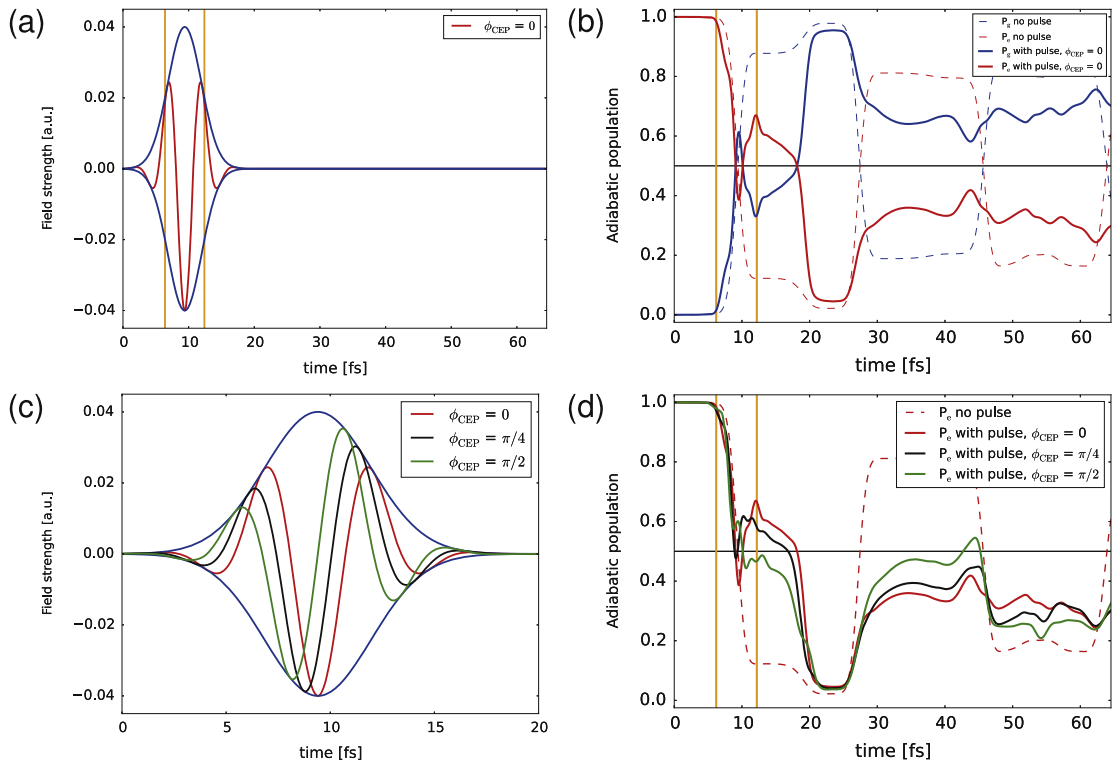

Figure 4. Field-modified population dynamics. (a) Control pulse with wavelength λ= 1600 nm, peak intensity $I_0 = 5.6 \times 10^{13}$ W cm^{-2}, FWHM 6 fs. (b) Population evolution of ground (blue) and excited adiabatic state (red) without pulse (dashed lines) and with the pulse shown in panel (a) (solid lines). The population dynamics are significantly modified by the laser pulse. (c) Same control pulses as in (a), but with different carrier-envelope phases ϕ_{CEP}:$\phi_{CEP} = 0$ (red), $\phi_{CEP} = \pi/4$ (black), $\phi_{CEP} = \pi/2$ (green). (d) Population evolution of excited adiabatic state without pulse (red dashed line) and with the pulse shown in panel (c) with $\phi_{CEP} = 0$ (red solid line), $\phi_{CEP} = \pi/4$ (black solid line), $\phi_{CEP} = \pi/2$ (green solid line), respectively. The population dynamics are CEP dependent. The vertical orange lines in (a), (b), (d) highlight the start and end time of the first (field-free) CI passage.

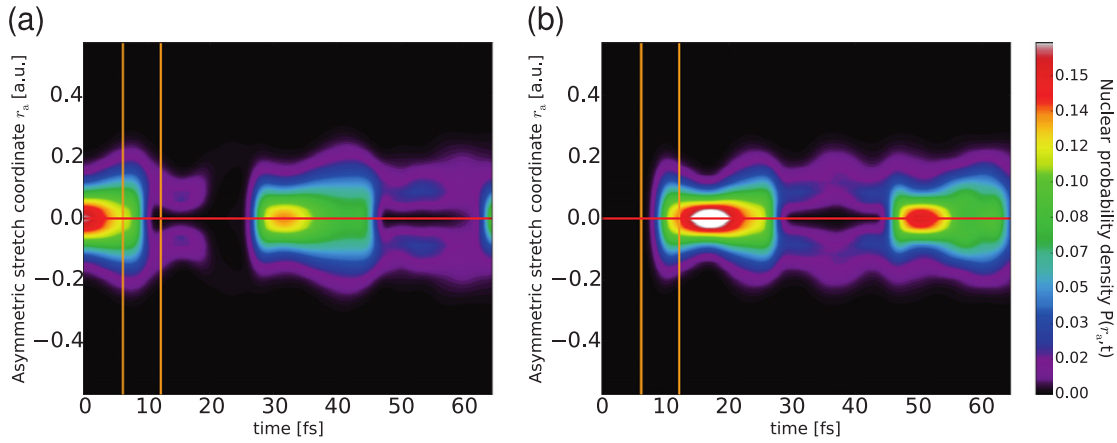

Figure 5. Field-free nuclear probability density evolution on the upper (a) and lower adiabatic surface (b) integrated over the bending angle θ as a function of the asymmetric stretch coordinate r_a. The vertical orange lines highlight the start and end time of the first CI passage. The horizontal red line indicates $r_a = 0$ a.u..

Let us start with panel (a): at $t = 0$ fs, the initial probability density is that of the lowest vibrational state of the electronic ground state, in accordance with the chosen initial conditions. Panel (a) shows that, while propagating along the reaction coordinate θ towards the CI, the wave packet spreads just a little along the asymmetric stretch coordinate r_a. At $t \sim 6$ fs, the nuclear wave packet has reached the CI region and the first non-adiabatic transition takes place, apparent by the emergence of the substantial nuclear probability density on the lower adiabatic surface, see panel (b). Note that the part of the nuclear wave packet that remains on the upper surface

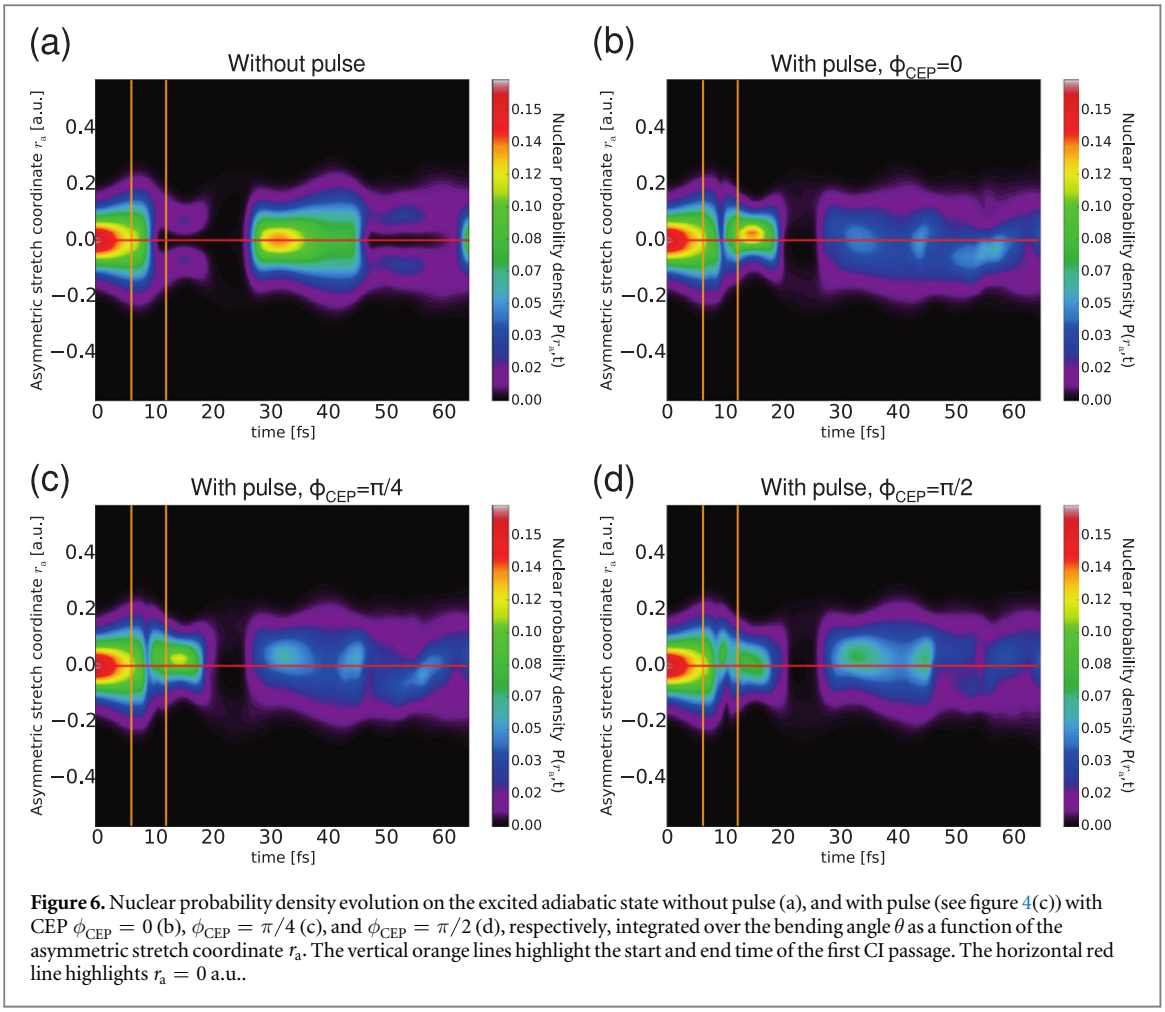

Figure 6. Nuclear probability density evolution on the excited adiabatic state without pulse (a), and with pulse (see figure 4(c)) with CEP $\phi_{CEP} = 0$ (b), $\phi_{CEP} = \pi/4$ (c), and $\phi_{CEP} = \pi/2$ (d), respectively, integrated over the bending angle θ as a function of the asymmetric stretch coordinate r_a. The vertical orange lines highlight the start and end time of the first CI passage. The horizontal red line highlights $r_a = 0$ a.u..

develops a node at $r_a = 0$ a.u. after passing the CI[7]; a signature of destructive self-interference of the wave packet due to the geometric phase effect [148–152]. At $t \sim 15$ fs, the part of the wave packet still evolving on the upper surface after the first CI passage, reaches its turning point. There it gets compressed, explaining the increase of the probability density. Shortly after that, the nuclear wave packet re-encounters the CI, resulting in the further increase of the ground state population around $t \sim 18.5$ fs, see figure 3(b). After this second CI passage, the population of the excited state is only ~5%, and, consequently, panel (a) shows virtually no nuclear probability density from $t \sim 20$ to $t \sim 25$ fs.

Let us turn to panel (b): at $t \sim 17$ fs, the part of the nuclear wave packet, which propagates on the lower surface, reaches its turning point, clearly evident from the substantial increase of the nuclear probability density around $r_a = 0$ a.u.. Then, 8 fs later (t ~ 25 fs), the wave packet reaches the CI, where we can observe another strong non-adiabatic transition, this time into the excited adiabatic state. Again, we can see the formation of a node due to the geometric phase effect in that part of the wave packet, which remains on the same surface when passing the CI region, here, on the lower adiabatic surface.

How do these wave packet dynamics change in the presence of the control pulse? Figure 6 shows the evolution of the nuclear probability density corresponding to the excited adiabatic state with and without the control pulse included in the calculations, and for the different CEP values of the pulse shown in figure 4(c).

Let us first focus on the time interval from $t = 0$ to $t = 20$ fs, when the pulse is acting on the molecule. We note that the CI dynamics have dramatically changed under the influence of the pulse and that the nodal structure, which is apparent in the field-free case (panel (a)), does not emerge (independently of the CEP). As the formation of the node is a consequence of the geometric phase effect at the CI [148–152], the absence of the nodal structure can be understood in terms of a considerable change of the CI region caused by the control pulse: The strong laser field changes the shapes of the PESs, in particular in the coupling region, in a way similar to the observations that have been made in prior studies.

[7] Note that the plotted probability density is integrated with respect to the bending angle θ, so that the instant of time at which the node becomes apparent in the figure is not identical to the instant of time when the leading edge of the wave packet encounters the CI, but rather when the entire part of the wave packet remaining on the upper surface has passed the coupling region.

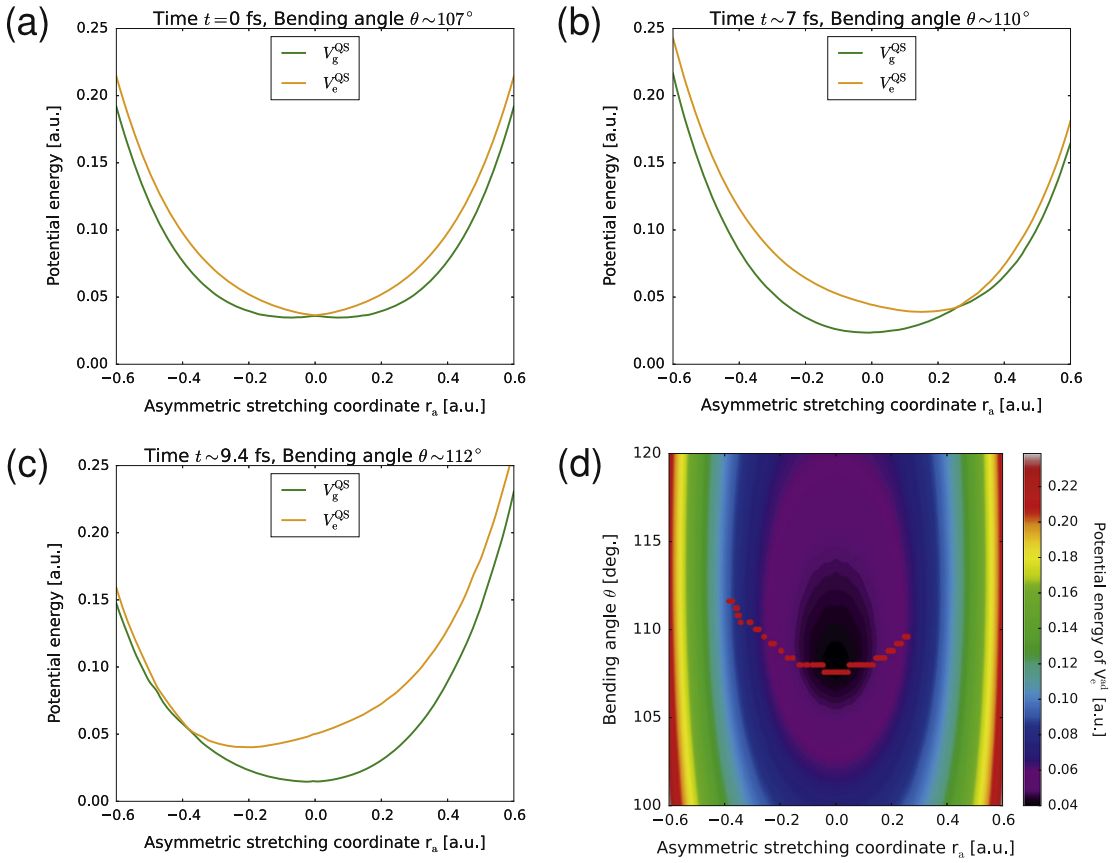

Figure 7. Laser-modified coupling region. (a)–(c) Cuts of laser-induced, quasistatic potential energy surfaces (PESs) along the coupling coordinate r_a for different bending angles θ and instants of time during the pulse (see figure 4(c)): (a) $\theta \sim 107°$ and $t = 0$ fs, (b) $\theta \sim 110°$ and $t \sim 7$ fs, and (c) $\theta \sim 112°$ and $t \sim 9.4$ fs. The cuts are taken at those angles θ, at which the laser-modified PESs touch. (d) The red dots on the PES of the (field-free) excited adiabatic state indicate the trajectory of the intersection position during the control pulse as a function of the nuclear coordinates r_a and θ.

In order to visualize the reshaping of the PESs, we have calculated the laser-induced quasistatic PESs by diagonalizing the time-dependent matrix $\boldsymbol{Q}^{\mathrm{d}}(t) = \boldsymbol{V}^{\mathrm{d}} + \boldsymbol{W}^{\mathrm{d}}(t)$, composed of the diabatic potential energy matrix $\boldsymbol{V}^{\mathrm{d}}$ and the time-dependent laser coupling matrix $\boldsymbol{W}^{\mathrm{d}}$ (see section 2.2). The laser-induced quasistatic PESs, $V_i^{\mathrm{QS}}(t)$ with $i = \{\mathrm{g,e}\}$, are the eigenvalues of $\boldsymbol{Q}^{\mathrm{d}}$ calculated for each instant of time. We find that using such instantaneous basis and the instantaneous transformation of the PES landscape allows for an intuitive and clear interpretation of our results.

Let us first consider the case, in which the CEP of the control pulse is $\phi_{\mathrm{CEP}} = 0$. Figure 7 shows cuts of the laser-induced, quasistatic PESs, V_i^{QS} with $i = \{g, e\}$, along the coupling coordinate r_a for different values of the bending angle θ and for different instants of time during the pulse (see figure 4(c)): (i) just before the turn-on of the pulse at $t = 0$ fs (panel (a)), (ii) when the field strength reaches its first positive maximum at $t \sim 7$ fs (panel (b)), and (iii) when the field strength reaches its negative maximum (equivalent to its peak value) at $t \sim 9.4$ fs (panel (c)). It is important to note that the cuts were taken at those values of the bending angle θ, at which the laser-modified PESs touch.

Panel (a) corresponds to the case when the laser pulse is off. Therefore the position of the intersection is identical to that of the CI in the field-free case, i.e., at $r_a = 0$ a.u. and $\theta \sim 107°$. At $t \sim 7$ fs, when the electric field strength is $E \sim +0.025$ a.u., the position of the intersection has changed to $r_a \sim +0.27$ a.u. and $\theta \sim 110°$. At $t \sim 9.4$ fs, the electric field strength is $E \sim -0.04$ a.u. and the position of the intersection has moved to $r_a \sim -0.39$ a.u. and $\theta \sim 112°$.

The red dots in panel 7(d) indicate the entire trajectory that the intersection position follows while the laser pulse is acting on the system, as a function of the nuclear coordinates r_a and θ. Following the field's oscillations, the position of the intersection 'swings' between positive and negative values of the asymmetric stretch coordinate r_a, depending on the sign of the electric field. The larger the absolute value of the field strength, the greater the displacement of the intersection with respect to $r_a = 0$ a.u. The same applies to the shift of the

intersection geometry with respect to the bending angle θ, however, the shift occurs only towards larger angles compared to the field-free CI geometry, $\theta_{CI} \sim 107°$.

The position of the moving intersection is determined by the elements of both the diabatic potential energy matrix $\boldsymbol{V}^{d}$ and the laser coupling matrix $\boldsymbol{W}^{d}(t)$, and, in particular, their symmetry properties with respect to the nuclear coordinates. All these matrix elements are either symmetric or antisymmetric with respect to the coupling mode r_a. In this study, we found that the transition dipole moment (in y direction) makes the most significant contribution to the change of the topological landscape of the coupling region. Based on the behavior of the intersection trajectory corresponding to the pulse with $\phi_{CEP} = 0$ (panel (d)) and the circumstance that the transition dipole moment is symmetric with respect to $r_a = 0$ a.u., we can easily predict the behavior of the trajectories caused by the pulses with different CEP. For a CEP of $\phi_{CEP} = \pi$, the sign of the electric field is inverted. In this case, the trajectory will be mirror-symmetric with respect to $r_a = 0$ a.u. to the $\phi_{CEP} = 0$ trajectory. For a CEP of $\phi_{CEP} = \pi/2$, where the absolute value of the maximum and minimum of the field strength is equal (see figure 4(c)), the entire trajectory is symmetric with respect to $r_a = 0$ a.u.. We stress that this analysis is based on the negligible contribution of the permanent dipole moments of the two states, which are antisymmetric with respect to the coupling mode r_a.

Let us now return to the interpretation of the nuclear probability densities shown in figure 6. The initial nuclear wave packet has even symmetry with respect to $r_a = 0$ a.u., which is retained until it reaches the CI region for the first time.

In the field-free case, the CI is located at $r_a = 0$ a.u., which means that the part of the nuclear wave packet that passes the CI region on 'one side' of the CI ($r_a > 0$) is equal to that propagating on 'the other side' of the CI ($r_a < 0$). In accordance with the geometric phase effect, the two parts that propagate along the different paths acquire a phase shift of $+\pi/2$ and $-\pi/2$, respectively. Hence, behind the CI, at $r_a = 0$ a.u. they interfere destructively and the wave packet acquires a node.

However, in the presence of the laser pulse, the CI region is subject to significant laser-induced reshaping while the nuclear wave packet is passing it. As a result, the wave packet does not experience the static CI at $r_a = 0$ a.u. while (mainly) propagating along $r_a = 0$ a.u. towards smaller bending angles θ. But, instead, the intersection, which is moving primarily perpendicular to the wave packet (between $r_a \sim -0.3$ a.u. and $r_a \sim +0.4$ a.u. around $\theta \sim 110°$, see figure 7(d)), 'cuts sideways' into it, sculpting it in the coordinate and momentum space. To illustrate this dynamic process, we have included a movie in the supplementary material, presenting the nuclear wave packet dynamics on the upper surface, as well as the trajectory of the moving intersection.

Since the intersection trajectory varies with the CEP, the wave packet passage through the CI region is sensitive to the CEP of the control pulse, explaining the differences apparent in the panels 6(b)–(d) for the time interval from $t \sim 6$ to $t \sim 12$ fs. The different evolution of the nuclear probability densities illustrates clearly how the 'moving intersection' sculpts the nuclear wave packet differently, depending on the pulse's CEP.

Let us turn our attention to the ensuing nuclear probability density evolution from $t = 20$ to $t = 65$ fs, long after the end of the laser pulse. We can see that the subsequent evolution of the nuclear wave packet, including further (field-free) passages through the CI, retains the memory of the control pulse and its CEP. Both the shapes of the nuclear wave packets at each PES and the relative phase between them, determined by the interaction with the ultrashort pulse during the first CI passage, control the field-free dynamics on the many tens of femtosecond time scale.

Figure 6 illustrates how the laser-controlled re-shaping of the nuclear wave packet during the first CI passage breaks the symmetry of the wave packet with respect to the coupling mode r_a. The 'rocking' time-dependent laser-dressed quasistatic PESs, see panels 7(a)–(c), drive the nuclear wave packet, which in the field-free case propagates symmetrically to $r_a = 0$ a.u., on an oscillatory trajectory around $r_a = 0$ a.u.. In other words, the modification of the coupling region is accompanied by momentum 'kicks' from the control pulse perpendicular to the main propagation direction of the wave packet. As a result, no nodal structure emerges in the nuclear probability densities shown in panels 6(b)–(d) for $t > 25$ fs. In fact, for $t > 18$ fs the field-free static CI is present, however, following its oscillatory trajectory, the nuclear wave packet no longer approaches the CI region 'symmetrically'.

In the limiting case of laser fields with periods much longer compared to the CI passage time of the nuclear wave packet, investigated by Arasaki *et al* in [67, 68], the intersection can be 'moved away' from its field-free position for the entire (ultrashort) passage time. In this situation the wave packet can 'miss' the coupling region almost fully, depending on the strength of the field.

4. Conclusions

Using the example of the NO_2 molecule (in restricted dimensionality), we have analyzed the possibility of sub-laser-cycle control of nuclear motion through the CI. We have found that adjusting the cycle of the control laser

pulse to the charateristic transit time through the CI leads to a dramatic modification of the wave packet dynamics, sensitive to the CEP of the control pulse. First, the motion of the CI induced by the control pulse sculpts the wave packets on both PESs and controls the branching ratio on the sub-cycle time scale. Second, the modifications of the wave packets on the coupled PESs, and in particular the altered electronic coherence between them, affect the further motion through the CI long after the control pulse is over. A similar re-shaping of the wave packet at the CI region can also be achieved by using a pulse with another near- or MIR laser wavelength (such as an 800 nm pulse), however, a *well-controlled* laser-induced re-shaping requires the application of a control pulse with a period that is comparable to the characteristic time of the CI passage of the nuclear wave packet. In this case, the sub-laser-cycle control of the introduced modifications is maximized.

The changes in the wave packet dynamics stimulated by the control pulse can be monitored by means of femtosecond time-resolved photoelectron spectroscopy [153], an established experimental technique for measuring excited state dynamics in polyatomic molecules, including ultrafast non-adiabatic processes [154]. The photoelectron angular distributions measured with standard femtosecond laser pulses and velocity map imaging techniques can be compared with theoretical predictions obtained with extended wave packet dynamics simulations including the interaction with the ionizing probe pulse and geometry- and energy-dependent photoionization matrix elements. High-harmonic spectroscopy constitutes another sensitive measuring technique, where the wave packet dynamics is encoded in the high-harmonic radiation emitted at different time delays upon excitation [155]. Both methods, and their more sophisticated counterparts such as femtosecond time-resolved photoelectron-photoion coincidence imaging, have already been used in the past to study both experimentally and theoretically the wave packet dynamics at the $1^2A_1/1^2B_2$ CI of NO_2, see e.g. [68, 80–83, 85, 87–89].

In this work, we have considered a reduced-dimensionality model. How would the full 3D nature of the dynamics affect the proposed control mechanism? In 2D, the CI is a single point, while in 3D it is a 1D seam of C_{2v} geometry. According to Mahapatra *et al* (see figure 1(a) in [75]), the CI seam depends weakly on the symmetric stretch coordinate, i.e., for varying r_s, it varies little with respect to the bending angle θ. Thus, for all relevant symmetric stretch components, the CI seam will be reached by the wave packet synchronously. As the laser-controlled CI slices through the wave packet mainly along the asymmetric stretch coordinate, it should happen virtually simultaneously for all relevant r_s. In general, as long as such synchronization is much better than 0.5 of the laser cycle, the proposed control mechanism should remain unaffected.

Acknowledgments

We would like to thank David Lauvergnat for valuable discussions. This work has been financially supported by the ERA-Chemistry Project PIM2010EEC-00751, DFG SM 292/3-1, the EU FP7 Marie Curie ITN CORINF, the EPSRC Programme Grant No. EP/I032517/1, the European Research Council Advanced Grant No. XCHEM 290853, the MINECO projects FIS2013-42002-R and CTQ2012-35513-C02, a MINECO FPU grant (LMF), the European COST Action XLIC CM1204, and the CAM project NANOFRONTMAG, which are gratefully acknowledged. We also acknowledge allocation of computer time from Mare Nostrum BSC and CCC-UAM.

References

[1] Brumer P and Shapiro M 1986 *Chem. Phys. Lett.* **126** 541–6
[2] Shapiro M, Hepburn J W and Brumer P 1988 *Chem. Phys. Lett.* **149** 451–4
[3] Tannor D J and Rice S A 1985 *J. Chem. Phys.* **83** 5013–8
[4] Tannor D J, Kosloff R and Rice S A 1986 *J. Chem. Phys.* **85** 5805–20
[5] Gaubatz U, Rudecki P, Becker M, Schiemann S, Külz M and Bergmann K 1988 *Chem. Phys. Lett.* **149** 463–8
[6] Gaubatz U, Rudecki P, Schiemann S and Bergmann K 1990 *J. Chem. Phys.* **92** 5363–76
[7] Bergmann K, Vitanov N V and Shore B W 2015 *J. Chem. Phys.* **142** 170901
[8] Shi S, Woody A and Rabitz H 1988 *J. Chem. Phys.* **88** 6870–83
[9] Kosloff R, Rice S, Gaspard P, Tersigni S and Tannor D 1989 *Chem. Phys.* **139** 201–20
[10] Dahleh M, Peirce A P and Rabitz H 1990 *Phys. Rev.* A **42** 1065–79
[11] Judson R S and Rabitz H 1992 *Phys. Rev. Lett.* **68** 1500–3
[12] Worth G A and Sanz C S 2010 *Phys. Chem. Chem. Phys.* **12** 15570–9
[13] Assion A, Baumert T, Bergt M, Brixner T, Kiefer B, Seyfried V, Strehle M and Gerber G 1998 *Science* **282** 919–22
[14] Weinacht T C, White J L and Bucksbaum P H 1999 *J. Phys. Chem.* A **103** 10166–8
[15] Levis R J, Menkir G M and Rabitz H 2001 *Science* **292** 709–13
[16] Brixner T and Gerber G 2003 *Chem. Phys. Chem.* **4** 418–38
[17] Worth G A and Cederbaum L S 2004 *Annu. Rev. Phys. Chem.* **55** 127–58
[18] Domcke W *et al* (ed) 2004 *Conical Intersections: Electronic Structure, Dynamics and Spectroscopy* (*Advanced Series in Physical Chemistry* vol 15) (New Jersey: World Scientific)
[19] Domcke W, Yarkony D R and Köppel H 2011 *Conical Intersections: Theory, Computation and Experiment* (*Advanced Series in Physical Chemistry* vol 17) (New Jersey: World Scientific)

[20] Herek J L, Wohlleben W, Cogdell R J, Zeidler D and Motzkus M 2002 *Nature* **417** 533–5
[21] Großmann F, Feng L, Schmidt G, Kunert T and Schmidt R 2002 *Europhys. Lett.* **60** 201–6
[22] Geppert D, Hofmann A and de Vivie-Riedle R 2003 *J. Chem. Phys.* **119** 5901–6
[23] Geppert D, Seyfarth L and de Vivie-Riedle R 2004 *Appl. Phys.* B **79** 987–92
[24] Mitrić R, Hartmann M, Pittner J and Bonačić-Koutecký V 2002 *J. Phys. Chem.* B **106** 10477–81
[25] Abe M, Ohtsuki Y, Fujimura Y and Domcke W 2005 *J. Chem. Phys.* **123** 144508
[26] Abe M, Ohtsuki Y, Fujimura Y, Lan Z and Domcke W 2006 *J. Chem. Phys.* **124** 224316
[27] Schneider R and Domcke W 1988 *Chem. Phys. Lett.* **150** 235–42
[28] Stock G and Domcke W 1993 *J. Phys. Chem.* **97** 12466–72
[29] Worth G A, Meyer H and Cederbaum L S 1996 *J. Chem. Phys.* **105** 4412–26
[30] Raab A, Worth G A, Meyer H D and Cederbaum L S 1999 *J. Chem. Phys.* **110** 936–46
[31] Ferretti A, Lami A and Villani G 1995 *Chem. Phys.* **196** 447–54
[32] Wang L, Meyer H D and May V 2006 *J. Chem. Phys.* **125** 014102
[33] Penfold T J, Worth G A and Meier C 2010 *Phys. Chem. Chem. Phys.* **12** 15616–27
[34] Thanopulos I, Li X, Brumer P and Shapiro M 2012 *J. Chem. Phys.* **137** 064111
[35] Sukharev M and Seideman T 2004 *Phys. Rev. Lett.* **93** 093004
[36] Sukharev M and Seideman T 2005 *Phys. Rev.* A **71** 012509
[37] Christopher P S, Shapiro M and Brumer P 2005 *J. Chem. Phys.* **123** 064313
[38] Christopher P S, Shapiro M and Brumer P 2006 *J. Chem. Phys.* **125** 124310
[39] Frishman E and Shapiro M 2001 *Phys. Rev. Lett.* **87** 253001
[40] Frishman E and Shapiro M 2003 *Phys. Rev.* A **68** 032717
[41] García-Vela A 2012 *J. Chem. Phys.* **136** 134304
[42] Dietrich P and Corkum P B 1992 *J. Chem. Phys.* **97** 3187–98
[43] Charron E, Giusti-Suzor A and Mies F H 1995 *Phys. Rev. Lett.* **75** 2815–8
[44] Thachuk M and Wardlaw D M 1995 *J. Chem. Phys.* **102** 7462–71
[45] Seideman T, Ivanov M Y and Corkum P B 1995 *Phys. Rev. Lett.* **75** 2819–22
[46] Zuo T and Bandrauk A D 1995 *Phys. Rev.* A **52** R2511–4
[47] Dietrich P, Ivanov M Y, Ilkov F A and Corkum P B 1996 *Phys. Rev. Lett.* **77** 4150–3
[48] Ivanov M, Matusek D and Wright J 1996 *Chem. Phys. Lett.* **255** 232–7
[49] Ivanov M Y, Matusek D R and Wright J S 1996 *Phys. Rev.* A **54** 5159–70
[50] Thachuk M, Ivanov M Y and Wardlaw D M 1996 *J. Chem. Phys.* **105** 4094–104
[51] Thachuk M, Ivanov M Y and Wardlaw D M 1998 *J. Chem. Phys.* **109** 5747–60
[52] Corkum P B, Ivanov M Y and Wright J S 1997 *Annu. Rev. Phys. Chem.* **48** 387–406
[53] Underwood J G, Spanner M, Ivanov M Y, Mottershead J, Sussman B J and Stolow A 2003 *Phys. Rev. Lett.* **90** 223001
[54] Sussman B J, Ivanov M Y and Stolow A 2005 *Phys. Rev.* A **71** 051401
[55] Sussman B J, Townsend D, Ivanov M Y and Stolow A 2006 *Science* **314** 278–81
[56] Marquetand P, Richter M, González-Vázquez J, Sola I and González L 2011 *Faraday Discuss.* **153** 261–73
[57] Sanz-Sanz C, Richings G W and Worth G A 2011 *Faraday Discuss.* **153** 275–91
[58] González-Vázquez J, Sola I R, Santamaria J and Malinovsky V S 2006 *Chem. Phys. Lett.* **431** 231–5
[59] González-Vázquez J, González L, Sola I R and Santamaria J 2009 *J. Chem. Phys.* **131** 104302
[60] Chang B Y, Shin S, Santamaria J and Sola I R 2009 *J. Chem. Phys.* **130** 124320
[61] Chang B Y, Shin S and Sola I R 2009 *J. Chem. Phys.* **131** 204314
[62] Kinzel D, Marquetand P and González L 2012 *J. Phys. Chem.* A **116** 2743–9
[63] Richings G W and Worth G A 2012 *J. Phys. Chem.* B **116** 11228–40
[64] Sala M, Saab M, Lasorne B, Gatti F and Guérin S 2014 *J. Chem. Phys.* **140** 194309
[65] Saab M, Sala M, Lasorne B, Gatti F and Guérin S 2014 *J. Chem. Phys.* **141** 134114
[66] Kling M F, von den Hoff P, Znakovskaya I and de Vivie-Riedle R 2013 *Phys. Chem. Chem. Phys.* **15** 9448–67
[67] Arasaki Y and Takatsuka K 2010 *Phys. Chem. Chem. Phys.* **12** 1239–42
[68] Arasaki Y, Wang K, McKoy V and Takatsuka K 2011 *Phys. Chem. Chem. Phys.* **13** 8681–9
[69] Han Y C, Yuan K J, Hu W H and Cong S L 2009 *J. Chem. Phys.* **130** 044308
[70] Scheit S, Arasaki Y and Takatsuka K 2012 *J. Phys. Chem.* A **116** 2644–53
[71] Scheit S, Arasaki Y and Takatsuka K 2014 *J. Chem. Phys.* **140** 244115
[72] Znakovskaya I *et al* 2012 *Phys. Rev. Lett.* **108** 063002
[73] Haller E, Köppel H and Cederbaum L 1985 *J. Mol. Spectrosc.* **111** 377–97
[74] Mahapatra S, Köppel H and Cederbaum L S 1999 *J. Chem. Phys.* **110** 5691–701
[75] Mahapatra S, Köppel H, Cederbaum L, Stampfuss P and Wenzel W 2000 *Chem. Phys.* **259** 211–26
[76] Santoro F and Petrongolo C 1999 *J. Chem. Phys.* **110** 4419–27
[77] Santoro F, Petrongolo C, Granucci G and Persico M 2000 *Chem. Phys.* **259** 193–200
[78] Kurkal V, Fleurat-Lessard P and Schinke R 2003 *J. Chem. Phys.* **119** 1489–501
[79] Sanrey M and Joyeux M 2006 *J. Chem. Phys.* **125** 014304
[80] Eppink A T J B, Whitaker B J, Gloaguen E, Soep B, Coroiu A M and Parker D H 2004 *J. Chem. Phys.* **121** 7776–83
[81] Form N T, Whitaker B J, Poisson L and Soep B 2006 *Phys. Chem. Chem. Phys.* **8** 2925–32
[82] Arasaki Y and Takatsuka K 2007 *Chem. Phys.* **338** 175–85
[83] Vredenborg A, Roeterdink W G and Janssen M H M 2008 *J. Chem. Phys.* **128** 204311
[84] Schinke R, Grebenshchikov S and Zhu H 2008 *Chem. Phys.* **346** 99–114
[85] Arasaki Y, Takatsuka K, Wang K and McKoy V 2010 *J. Chem. Phys.* **132** 124307
[86] Wilkinson I and Whitaker B J 2010 *Annu. Rep. Prog. Chem.* **106** 274–304
[87] Wörner H J *et al* 2011 *Science* **334** 208–12
[88] Ruf H *et al* 2012 *J. Chem. Phys.* **137** 224303
[89] Kraus P M, Arasaki Y, Bertrand J B, Patchkovskii S, Corkum P B, Villeneuve D M, Takatsuka K and Wörner H J 2012 *Phys. Rev.* A **85** 043409
[90] Grein F 2008 *Chem. Phys. Lett.* **455** 124–30
[91] Reignier D, Stoecklin T, Halvick P, Voronin A and Rayez J C 2001 *Phys. Chem. Chem. Phys.* **3** 2726–34

[92] Salzgeber R F, Mandelshtam V, Schlier C and Taylor H S 1998 *J. Chem. Phys.* **109** 937–41
[93] Hirsch G and Buenker R J 1985 *Can. J. Chem.* **63** 1542–9
[94] Hirsch G, Buenker R J and Petrongolo C 1990 *Mol. Phys.* **70** 835–48
[95] Hirsch G, Buenker R J and Petrongolo C 1991 *Mol. Phys.* **73** 1085–99
[96] Hirsch G, Buenker R J and Petrongolo C 1992 *Mol. Phys.* **76** 1261–3
[97] Leonardi E and Petrongolo C 1997 *J. Chem. Phys.* **106** 10066–71
[98] Jackels C F and Davidson E R 1976 *J. Chem. Phys.* **64** 2908–17
[99] Jackels C F and Davidson E R 1976 *J. Chem. Phys.* **65** 2941–57
[100] Gillispie G D, Khan A U, Wahl A C, Hosteny R P and Krauss M 1975 *J. Chem. Phys.* **63** 3425–44
[101] Gillispie G D and Khan A U 1976 *J. Chem. Phys.* **65** 1624–33
[102] Grebenshchikov S Y, Beck C, Flöthman H, Schinke R and Kato S 1999 *J. Chem. Phys.* **111** 619–32
[103] Kaldor U 1990 *Chem. Phys. Lett.* **170** 17–20
[104] Kaldor U 1991 *Chem. Phys. Lett.* **185** 131–5
[105] Blahous III C P, Yates B F, Xie Y and Schaefer III H F 1990 *J. Chem. Phys.* **93** 8105–9
[106] Krebs S and Buenker R J 1995 *J. Chem. Phys.* **103** 5613–29
[107] Mota V C, Caridade P J S B and Varandas A J C 2011 *Int. J. Quantum Chem.* **111** 3776–85
[108] Mota V C, Caridade P J S B and Varandas A J C 2012 *J. Phys. Chem.* A **116** 3023–34
[109] Varandas A J C 2003 *J. Chem. Phys.* **119** 2596–613
[110] Xie Y, Davy R D, Yates B F, Blahous III C P, Yamaguchi Y and Schaefer III H F 1989 *Chem. Phys.* **135** 179–86
[111] Suzzi Valli G, Orrú R, Clementi E, Laganà A and Crocchianti S 1995 *J. Chem. Phys.* **102** 2825–32
[112] González M, Oliva C and Sayós R 2002 *J. Chem. Phys.* **117** 680–92
[113] Liévin J, Delon A and Jost R 1998 *J. Chem. Phys.* **108** 8931–43
[114] Sardar S, Mukherjee S, Paul A K and Adhikari S 2013 *Chem. Phys.* **416** 11–20
[115] Sayós R, Oliva C and González M 2001 *J. Chem. Phys.* **115** 1287–97
[116] Joyeux M, Jost R and Lombardi M 2003 *J. Chem. Phys.* **119** 5923–32
[117] Schinke R 2008 *J. Chem. Phys.* **129** 124303
[118] Bowman W C and de Lucia F C 1982 *J. Chem. Phys.* **77** 92–107
[119] Morino Y, Tanimoto M, Saito S, Hirota E, Awata R and Tanaka T 1983 *J. Mol. Spectrosc.* **98** 331–48
[120] Jost R, Nygard J, Pasinski A and Delon A 1996 *J. Chem. Phys.* **105** 1287–90
[121] Herzberg G 1991 *Molecular Spectra and Molecular Structure vol 3 Electronic Spectra and Electronic Structure of Polyatomic Molecules* (Malabar, FL: Krieger)
[122] Chase M W Jr, Davies C A, Downey J R Jr, Frurip D J, MacDonald R A and Syverud A N 1985 JANAF Thermochemical Tables 3rd Edition *J. Phys. Chem. Ref. Data* **14** (**Suppl 1**) (www.nist.gov/srd/monogr.cfm)
[123] Schryber J H, Polyansky O L, Jensen P and Tennyson J 1997 *J. Mol. Spectrosc.* **185** 234–43
[124] Brand J C D, Cross K J and Hoy A R 1979 *Can. J. Phys.* **57** 428–41
[125] Delon A, Jost R and Jacon M 2001 *J. Chem. Phys.* **114** 331–44
[126] Hardwick J L and Brand J C D 1976 *Can. J. Phys.* **54** 80–91
[127] Hardwick J and Brand J 1973 *Chem. Phys. Lett.* **21** 458–61
[128] Baer M 2006 *Beyond Born–Oppenheimer: Electronic Nonadiabatic Coupling Terms and Conical Intersections* (New Jersey: Wiley)
[129] Lischka H, Shepard R, Brown F B and Shavitt I 1981 *Int. J. Quantum Chem.* **20** 91–100
[130] Shepard R, Shavitt I, Pitzer R M, Comeau D C, Pepper M, Lischka H, Szalay P G, Ahlrichs R, Brown F B and Zhao J G 1988 *Int. J. Quantum Chem.* **34** 149–65
[131] Lischka H *et al* 2001 *Phys. Chem. Chem. Phys.* **3** 664–73
[132] Lischka H, Müller T, Szalay P G, Shavitt I, Pitzer R M and Shepard R 2011 *WIREs* **1** 191
[133] Lischka H *et al* 2012 *COLUMBUS, an ab initio electronic structure program, release 7.0* (www.univie.ac.at/columbus/)
[134] Császár P and Pulay P 1984 *J. Mol. Struct.* **114** 31–4
[135] Mead C A and Truhlar D G 1982 *J. Chem. Phys.* **77** 6090–8
[136] Baer M 2002 *Phys. Rep.* **358** 75–142
[137] Werner H J *et al* 2009 *MOLPRO, version 2009, a package of ab initio programs* (www.molpro.net)
[138] Simah D, Hartke B and Werner H J 1999 *J. Chem. Phys.* **111** 4523–34
[139] Richter M, Bouakline F, González-Vázquez J, Martínez-Fernández L, Corral I, Patchkovskii S, Morales F, Ivanov M, Martín F and Smirnova O 2015 in preparation
[140] Nauts A and Chapuisat X 1985 *Mol. Phys.* **55** 1287–318
[141] Lauvergnat D and Nauts A 2002 *J. Chem. Phys.* **116** 8560–70
[142] Gatti F and Iung C 2009 *Phys. Rep.* **484** 1–69
[143] Colbert D T and Miller W H 1992 *J. Chem. Phys.* **96** 1982–91
[144] Zhavoronkov N and Korn G 2002 *Phys. Rev. Lett.* **88** 203901
[145] Wirth A *et al* 2011 *Science* **334** 195–200
[146] Manzoni C, Mücke O D, Cirmi G, Fang S, Moses J, Huang S W, Hong K H, Cerullo G and Kärtner F X 2015 *Laser Photonics Rev.* **9** 129–71
[147] Luu T, Garg M, Kruchinin S Y, Moulet A, Hassan M T and Goulielmakis E 2015 *Nature* **521** 498–502
[148] Longuet-Higgins H C 1975 *Proc. R. Soc.* A **344** 147–56
[149] Mead C A and Truhlar D G 1979 *J. Chem. Phys.* **70** 2284–96
[150] Berry M V 1984 *Proc. R. Soc.* A **392** 45–57
[151] Mead C A 1992 *Rev. Mod. Phys.* **64** 51–85
[152] Yarkony D R 1996 *Rev. Mod. Phys.* **68** 985–1013
[153] Wollenhaupt M, Engel V and Baumert T 2005 *Annu. Rev. Phys. Chem.* **56** 25–56
[154] Stolow A, Bragg A E and Neumark D M 2004 *Chem. Rev.* **104** 1719–58
[155] Lein M 2007 *J. Phys. B: At. Mol. Opt. Phys.* **40** R135